CrossMark

Strain Behavior of Soil and Reinforcement in Wrap Faced Reinforced Soil Walls Subjected to Seismic Excitation

Arup Bhattacharjee · A. Murali Krishna

Abstract Behavior of reinforced soil structure depends mainly on strain mobilization within reinforcement and its surrounding soil. This paper presents the soil and reinforcement strains developed within wrap faced reinforced soil wall subjected to dynamic excitation and their interdependence on formation of deformation zones. Octahedral shear strains developed on backfill soil and axial strains in reinforcement during the dynamic excitation are determined from the numerical simulations and analyzed. In general, the octahedral strain increments during the dynamic excitation are more at higher elevations near the end of reinforcement and the reinforcement strain increments are lower at top layers. Parametric studies are also conducted to study behavior of soil strain and reinforcement strain for different reinforcement configurations and backfill materials. The octahedral shear strain increments and reinforcement strain increments are influenced by the longer reinforcement layers, more number of reinforcement layer and higher backfill friction angle. It is observed that at the lower elevations the soil strains and reinforcement strains were not significantly affected by change in reinforcement length. So providing longer reinforcements up to 1/3–1/2 the height of wall would yield better performance results.

A. Bhattacharjee (✉)
Department of Civil Engineering, Jorhat Engineering College, Jorhat, Assam, India
e-mail: bhatta_arup@yahoo.com

A. M. Krishna
Department of Civil Engineering, Indian Institute of Technology Guwahati, Guwahati, India
e-mail: amurali@iitg.ac.in

Notations

N_L	Number of reinforcement layers
γ_{oct}	Octahedral shear strain (%)
$\varepsilon_{xx}, \varepsilon_{yy}, \varepsilon_{zz}, \varepsilon_{xy},$ $\varepsilon_{yx}, \varepsilon_{zy}$	Six strain parameters in x, y and z directions
a	Acceleration (m/sec^2)
f	Frequency (Hz)
ε_a	Axial strain (%)
ϕ	Angle of internal friction (degree)
H	Height of wall (m)
L_{rein}	Reinforcement length (m)
$\Delta\varepsilon_{a\_rein}$	Incremental axial strain in reinforcement
$\Delta\gamma_{oct}$	Incremental octahedral shear strain

Introduction

Reinforced soil retaining structures are being used in place of conventional retaining structures extensively in the recent decades. Studies on seismic behavior of reinforced soil walls have been the interest of many researchers ([26], [25], [8], [5], [20], [9], [13–15], [17], [18], etc.). Such studies, mostly focused on accelerations, displacements and reinforcement loads/strain behavior of wrap/rigid faced or segmental reinforced soil walls. As numerical models that were validated with physical model observations facilitate extensive parametric analyses, few researchers developed numerical models to understand behavior of these structures ([3], [2, 19], [21], [27], [22] and [24] etc.).

Recently, Bhattacharjee and Murali Krishna [1] developed numerical model using FLAC^{3D} (Fast Lagrangian Analysis of Continua) to simulate the seismic behavior of wrap faced reinforced soil walls.

It is well known that the behavior of reinforced soil structure depends mainly on the level of strain mobilization in reinforcement materials which in turn depends on strain levels in the neighboring soil. To the authors' knowledge, very little was reported in the literature on the strain behavior of soil and reinforcement separately. In the present study, an attempt has been made to evaluate the soil and reinforcement strains and their inter dependence in wrap faced reinforced soil walls subjected to seismic excitation. For the purpose, numerical model developed and validated by Bhattacharjee and Murali Krishna [1] is considered for analyzing the octahedral shear strains within soil and axial strains in reinforcement using seismic excitation studies.
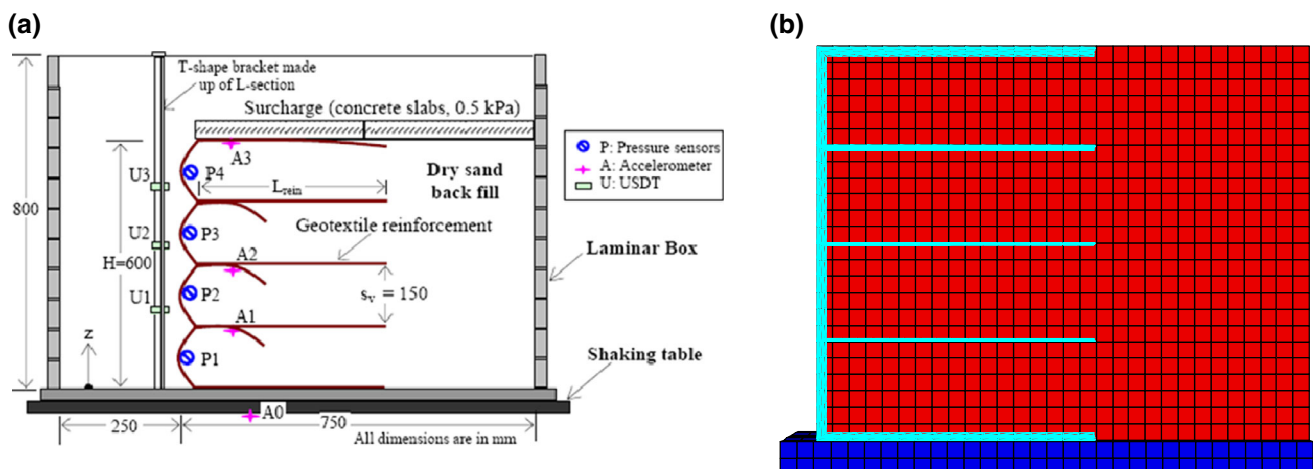
Numerical Model for Wrap Faced Reinforced Soil Walls

Target Physical Model

Physical model tests on wrap faced reinforced soil walls reported by Krishna and Latha [15] are considered for the development of numerical model. The target physical models tested on the shaking table were of size 750 mm × 500 mm in plan area and 600 mm (H) deep. The models were constructed in flexible laminar container using four layers of geotextile reinforcement of length (L_{rein}) 420 mm (i.e., 0.7 times the height as per [6]). The model was constructed in equal lifts of sand filling by pluviation method and geotextile reinforcement layers were wrapped around to

form facing (by folding the geotextile through 180° to form face and anchoring it to backfill) using a facing formwork. The backfill material used in the model tests was poorly graded sand having unit weight of about 16.2 kN/m^3 and friction angle of 45°. A 1 mm thick woven geotextile having mass per unit area of 230 gm/m^2 with about 50 kN/m breaking strength was used in the tests. A nominal surcharge of 0.5 kPa was applied after completion of all lifts of the wrapped wall and then the facing formwork was removed in sequence from bottom to top. After removing the supports, model wall was subjected to 20 cycles of sinusoidal motion at different frequencies. Results obtained through various instrumentations were discussed in terms of facing horizontal deformations, acceleration amplification values. The details of the test configuration and location of various instrumentations are shown in Fig. 1a.

Development of Numerical Model

A grid of size 600 mm height and 750 mm long is generated to represent the backfill of wrap faced retaining wall. A rigid zone of size 800 mm long and 50 mm thick considered at the base of wall to represent the shaking table. Initially model dimension in y direction is considered as single grid wide to represent the model wall in plane strain condition. Later on the lateral dimension is increased to observe the effect of lateral dimension on model response. The whole grid is divided into cubical brick elements of size 25 mm each. The size of grid are selected in such a way that, the mesh size of the model must be approximately smaller than one-tenth to one-eighth of the highest frequency component of the input wave for accurate transmission of wave through a model [16] during dynamic shaking. Figure 1b shows the numerical grid considered to simulate the wrap faced reinforced soil wall. The model is generated in same sequence as that of physical

(a)

(b)

Fig. 1 Test arrangement of wrap faced reinforced retaining wall **a** physical model tests (after [15]) **b** Numerical model (after [1]). (Color figure online)

model. Before placing the first layer of back fill, the foundation zone is generated and brought to static equilibrium. The model is generated in equal lifts with reinforcement wrapped around to form facing for each lift. The facing of the model is fixed in x direction to represent the facing support. The model is solved for static equilibrium after generation of grids of each lift. The supports are removed in sequence from top to bottom after building the wall up to full height and applying the surcharge pressure of 0.5 kPa. After support removal of each lift the model is solved for static equilibrium.

Material Properties

Material properties reported by Krishna and Latha [13, 15] and Bhattacharjee and Murali Krishna [1] are adopted in the present study and is listed in Table 1.

The backfill soil is modeled as elasto-plastic Mohr–Coulomb material coded with hyperbolic soil modulus proposed by Duncan et al. [4]. The stress dependent deformation modulus (E_t) expressed by the hyperbolic equation as

$$E_t = \left[1 - \frac{R_f(1 - \sin\phi)(\sigma_1 - \sigma_3)}{2(c.\cos\phi + \sigma_3 \sin\phi)} \right]^2 K_n.P_a \left(\frac{\sigma_3}{P_a} \right)^n \quad (1)$$

where K_n is the modulus number; n is the modulus exponent; c is the cohesion; σ_1 and σ_3 are the major and minor effective confining stress respectively; ϕ is the angle of internal friction; R_f is the failure ratio; p_a is atmospheric

Table 1 Material properties used in numerical model

Soil properties for Mohr model with stress dependent hyperbolic soil modulus parameters	
Mass density, kg/m^3	1,630
Elastic modulus, kPa	1×10^4
Poisson's ratio	0.3
Friction angles, degrees	38
Dilation angle, degree	10
Cohesion, kPa	0.1
Atmospheric pressure kPa	101.3
Modulus number, k	831
Modulus exponent, n	0.678
Failure ratio, R_f	0.9
Reinforcement (Geotextile) properties	
Mass density, kg/m^3	0.23
Thickness, m	0.001
Stiffness, kN/m	150
Reinforcement (Geotextile) interface properties	
Coupling spring cohesion, kPa	0.1
Coupling spring friction, Degrees	28
Coupling spring stiffness, kPa	1×10^6

pressure. The shear behavior of granular soils under cyclic loading is modeled using non-linear and hysteretic constitutive relation that follows the Massing rule [3] during unloading and reloading cycles. The tangent shear modulus during the first cycle is expressed as [1]:

$$G_t = \frac{G_{max}}{\left[1 + \left(\frac{G_{max}}{\tau_{max-oct}} \right) |\gamma_{\epsilon-oct}| \right]^2} \quad (2)$$

where G_{max} is the initial shear modulus, $\tau_{max-oct}$ is the maximum octahedral shear stress in three dimensional state which is related to shear parameters of soil through cohesion c and internal angle of friction ϕ, $\gamma_{\epsilon-oct}$ and is the octahedral shear strain. The tangent modulus during unloading/reloading cycle is

$$G_t = \frac{G_{max}}{\left[1 + \left(\frac{G_{max}}{2\tau_{max-oct}} \right) |\gamma_{\epsilon-oct} - \gamma_{r-oct}| \right]^2} \quad (3)$$

where (γ_{r-oct}, τ_{r-oct}) represents the octahedral stress state at which the shear stress reverses direction.

The geotextile reinforcement is modeled using geogrid structural element available in FLAC^{3D} for full width of the model. The geogrid elements are three nodded shell elements used to model flexible membrane that resist as membrane but do not resist bending loading. The effective confining stress and total shear stress developed on geogrid are balanced by the membrane stress developed within the geogrid itself [10]. Interface between dissimilar materials is modeled as linear spring-slider system. The interface behavior of geogrid is represented numerically at each geogrid node by a rigid attachment in normal direction and spring-slider in the tangent plane to the geogrid surface. The orientation of the spring-slider changes in response to the shear displacement between geogrid and neighboring soil elements [10]. The required input parameters for geogrid element and interface parameters are shown in Table 1. The geogrid structural element has interface friction angle of 28°, representing a rough surfaced reinforcement.

The boundary conditions applied to the model represent the actual boundary of the physical model tests. Bottom boundaries are completely fixed in vertical direction. The far end boundary elements are fixed in x direction. During the construction, the model wall is fixed in horizontal direction to represent the facing support. The lateral boundaries are fixed in y direction to represent the lateral boundaries at the side of the physical model. After the completion of all layers construction and the model was brought to equilibrium, the facing boundaries are removed stage by stage representing the stage wise removal of support. After the support removal the model is brought to equilibrium. During dynamic run the free field boundary is applied to far end. The constitutive model for soil is able to implement the damping of soil through the cyclic
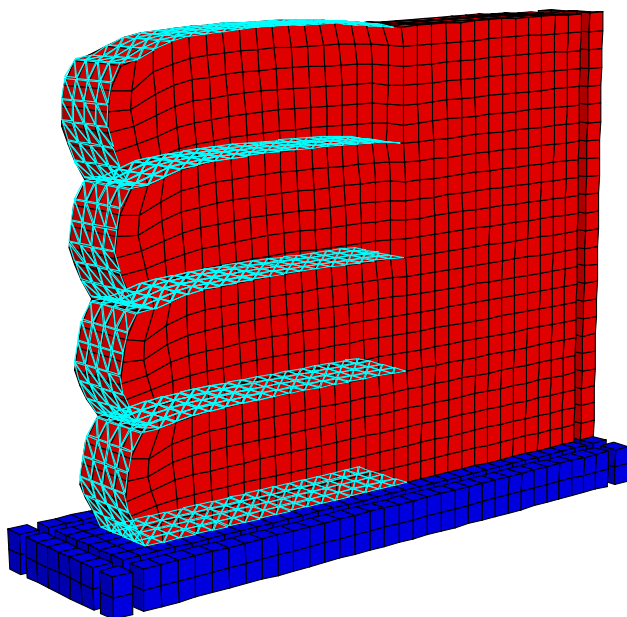
Fig. 2 Displaced model after dynamic simulation. (Color figure online)

hysteresis. However, local damping ratio of 5 % is adopted for soil element during dynamic analysis to simulate the properly the damping of soil when strain level is small ([21], [18], [23]).

The dynamic excitation is applied at the stiff bottom in the form of wave velocity in horizontal direction (uni-axial shaking). The displaced grid after dynamic excitation is shown in Fig. 2. During dynamic excitation, displacement histories are recorded at elevations of 200, 350 and 500 mm and acceleration histories at elevations 150, 300 and 600 mm to compare the results of physical model tests that were considered.

Validation of Numerical Model

Sinusoidal dynamic excitation of 0.2 g base acceleration (*a*) at different frequency (*f*) 3 and 5 Hz for 20 cycles are applied at the base of the model. Acceleration amplifications at different elevation of wall are quantified as *root mean square acceleration* (RMSA) amplification factor. The RMSA amplification factor is the ratio of RMS acceleration values at different elevation to that of base RMS acceleration value. The RMS acceleration value can be calculated according to Eq. 4 [12].

$$RMS = \left[\frac{1}{t_d} \int_0^{t_d} a(t)^2 dt \right]^{1/2} \tag{4}$$

where $a(t)$ is acceleration time history, t_d is the duration of the acceleration record and dt is time interval of the acceleration record.

Figure 3 compares the variation of horizontal displacements and RMSA amplification factors at different elevations obtained from physical test conducted and numerical model for acceleration 0.2 g at frequencies of 3 and 5 Hz. The maximum horizontal displacement at an elevation of 500 mm is 26.79 mm and that of physical model 30.08 mm for frequency of 3 Hz. The acceleration amplification at an elevation of 600 mm is 1.57 for numerical model and for physical model 1.71 for 3 Hz frequency. The results obtained show the ability of numerical model to capture the behavior of physical model.

Numerical model with different layer configurations are also subjected to dynamic excitation. Figure 4 shows the variation of horizontal displacements and RMSA amplification factors for different reinforcement layers configurations of physical and numerical simulations. The figure shows similar behavior of decreasing horizontal displacements with increase in reinforcing layers for both physical and numerical simulations. The RMSA amplification factors are not affected by variation of number of reinforcement layers. Figures 3 and 4 indicate the percentage errors in matching the experimental and numerical results in the range of 5 to 10 %. This show reasonable agreement of model behavior between physical and numerical model tests and confirm the validation of the numerical model.

Response of Full Scale Wrap Faced Reinforced Soil Wall Under Seismic Excitation

Typical height of retaining walls varies between 5 and 7 m for overpass and underpass as per the minimum vertical clearance requirements [11]. A 6 m high full scale model is considered for present analysis. To avoid the possible boundary effects on the model response near facing and within the reinforced zone, length of the backfill equal to three times the height of wall was adopted. Using the validated numerical model, a full scale wrap faced model of size 6 m high, 18 m long and 1 m wide with six layers of reinforcement (N_L) is studied for its seismic behavior. The model parameters are kept same as that of laboratory scale model, shown in Table 1. The model is subjected to 20 cycles of sinusoidal seismic excitation of 0.2 g acceleration at 5 Hz. The horizontal and vertical displacements near wall facing (0.5 m), at the end of reinforcement (4.2 m) and at deep backfill (14.0 m) after dynamic excitation are shown in Fig. 5. The deep backfill at 14 m is so chosen that, it is away from influence of the wall facing. The horizontal displacement decreases with the increase in distances from wall facing. The horizontal and vertical displacements are negligible at a distance of 14 m from wall facing. But the maximum vertical displacement at 5.5 m elevation is 61.7 mm near wall face, while near the
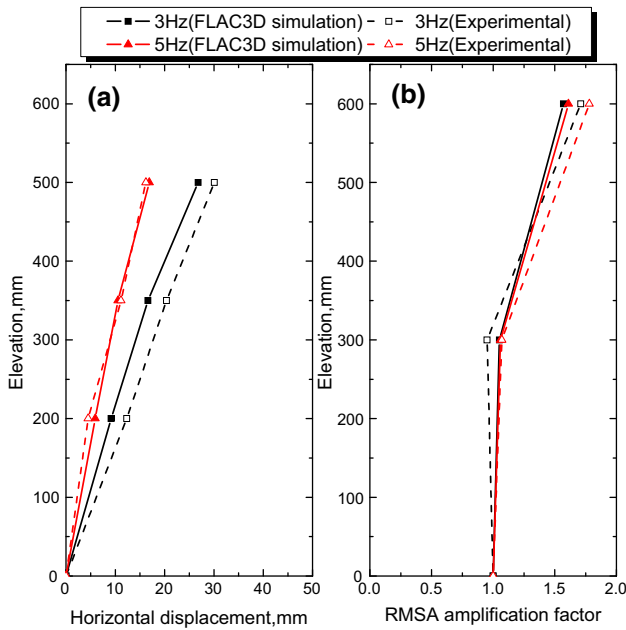
Fig. 3 Variation of horizontal displacement and RMSA amplification factor at different elevations ($a = 0.2$ g, $L_{rein}/H = 0.7$, $N_L = 4$)
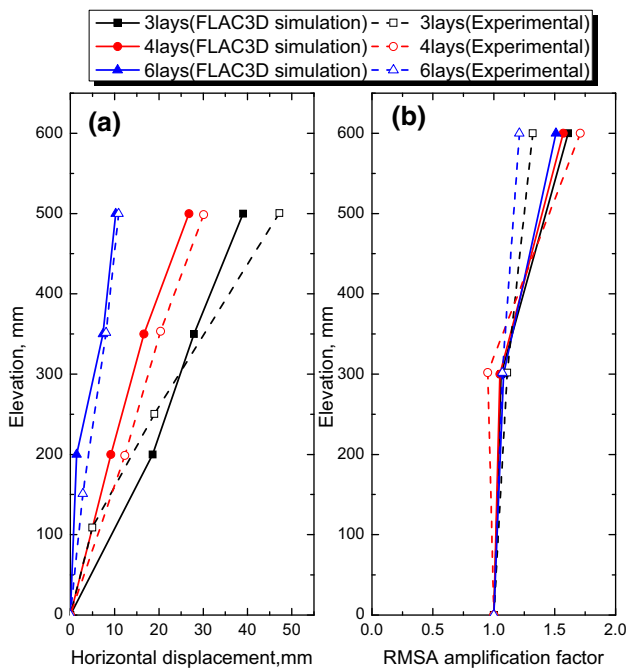
Fig. 4 Variation of horizontal displacements and RMSA amplification factors at different elevations ($a = 0.2$ g, $f = 3$ Hz, $L_{rein}/H = 0.7$) for model walls with different reinforcement layers

end of reinforcements it is 104.5 mm near end of reinforcement. The far end horizontal and vertical displacements are negligible. So the far field displacements will not have much effect on formation of deformation zones within and outside reinforced portion of wall.
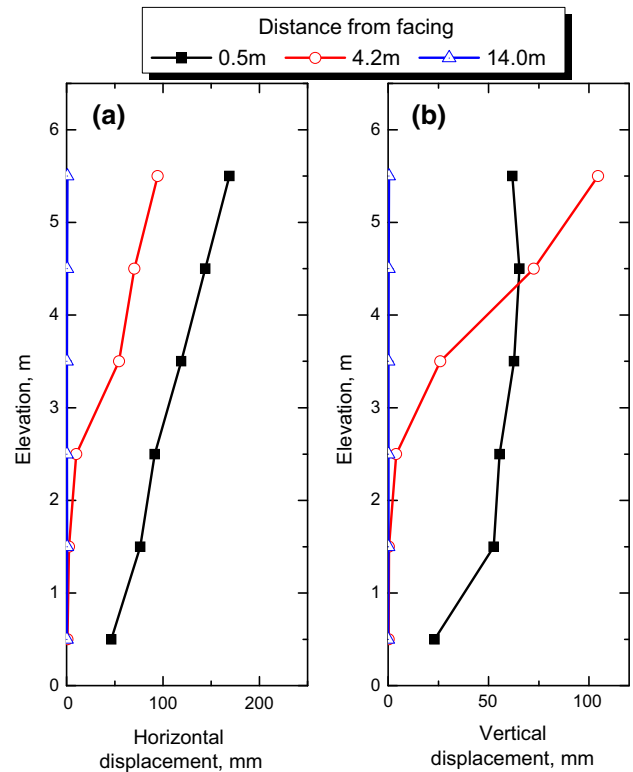
Fig. 5 Horizontal and vertical displacements of reinforced soil wall at different elevations after 20 cycles of dynamic excitation ($a = 0.2$ g, $L_{rein}/H = 0.7$, $N_L = 6$)

The incremental octahedral shear strains ($\Delta\gamma_{oct}$), horizontal and vertical displacements along the length of backfill, after the dynamic excitation, are presented in Fig. 6, to observe their effect on formation of deformation zones. The horizontal displacement of soil element near face of wall is 171.4 mm at an elevation of 5.5 m and remains constant up to 3.5 m from the face of wall. The horizontal displacement then decreases and become almost zero at 7 m from the face of wall. The vertical displacement of soil element is 69.8 mm near face of wall at that elevation. The vertical displacement remains almost constant up to 3.5 m from the face of wall. Then vertical displacement increase to 104.5 mm at a distance of 4.2 m from the face of wall. The incremental shear strain ($\Delta\gamma_{oct}$) near the face of wall is negligible and increases to 2.9 % at 2 m from face of wall at an elevation of 5.5 m. So from the Fig. 6, it is observed that the horizontal displacements of soil element within reinforced zone are maximum and they decrease gradually and become negligible after end of reinforcements at elevation of 5.5, 4.5, and 3.5 m. But at the lower layers i.e. 2.5 m and 1.5 m the horizontal movement of soil element decreases to zero within reinforced zone. The vertical settlements are almost uniform within reinforced zone i.e. up to a distance of 4 m from wall facing at an elevation of 5.5 m and 4.5 m. The vertical

Fig. 6 Incremental octahedral shear strain, horizontal displacement and vertical displacement along the length of backfill after 20 cycles of dynamic excitation ($a = 0.2$ g, $f = 5$ Hz, $L_{rein}/H = 0.7$, $N_L = 6$)
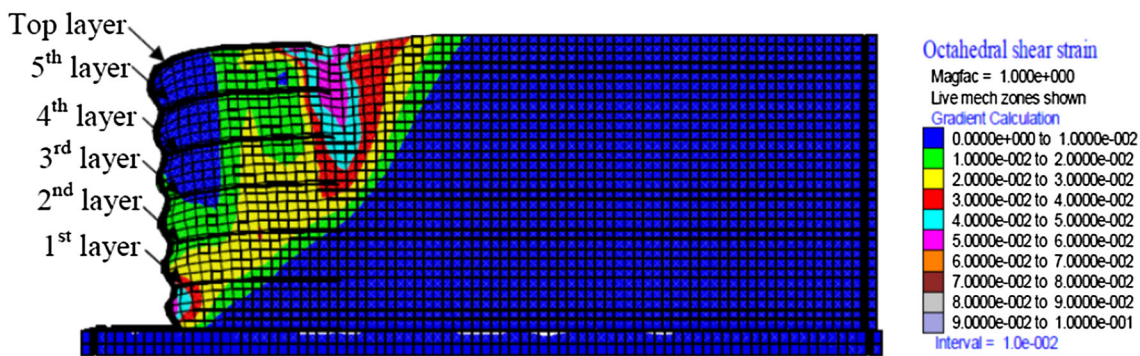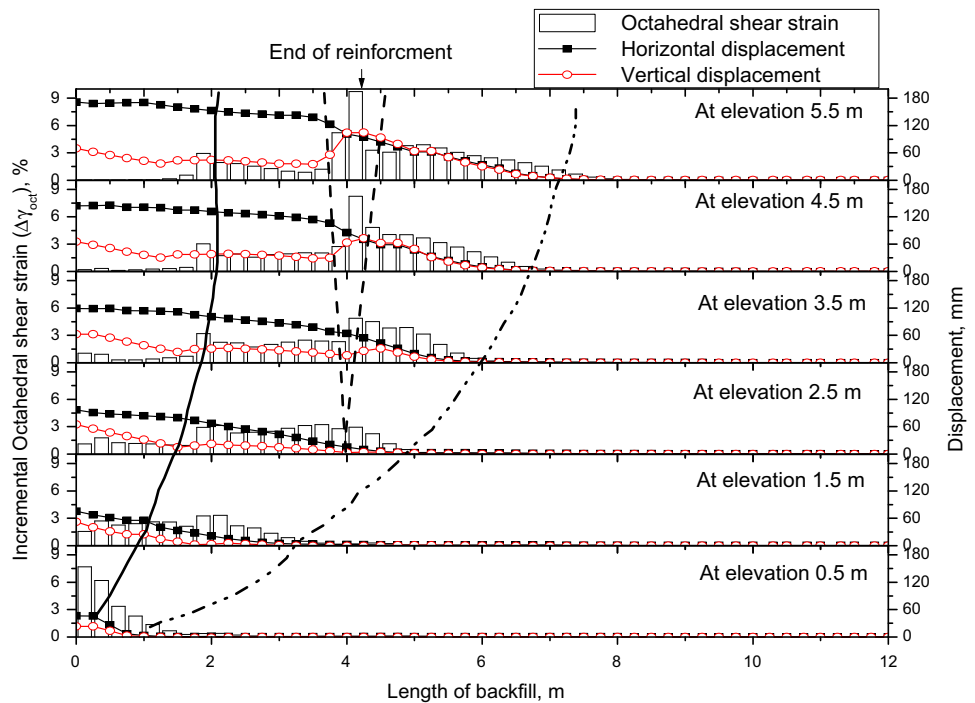

Fig. 7 Contour of octahedral shear strain after 20 cycles of dynamic excitation ($a = 0.2$ g, $f = 5$ Hz, $L_{rein}/H = 0.7$, $N_L = 6$). (Color figure online)

settlement increases suddenly near the end of reinforcement at higher layers i.e. at an elevation of 5.5 m and 4.5 m. The vertical settlements are lesser at lower layers i.e. at an elevation of 3.5, 2.5 and 1.5 m and decreases to zero within reinforced zone. The incremental octahedral shear strain ($\Delta\gamma_{oct}$) reaches peak within reinforced zone near end of reinforcement within reinforced zone and after end of reinforcement in backfill soil. By comparing the $\Delta\gamma_{oct}$, horizontal displacement and vertical settlement at different layers, it can be seen that the deformation of wrap faced wall subjected to dynamic excitation consist of three different modes: shear deformation within reinforced zone, relative compaction near end of reinforcement and shear zone extending to backfill zone. Figure 6 shows two deformations; one shear deformation zone within reinforced block (solid line) and other shear deformation zone extending beyond reinforced block (dashed-dotted line).

Besides these two deformation zones a zone of relative compaction (dashed line) can be observed at the end of reinforcement which is due to higher vertical settlements and shear strains. Similar deformation zones were also reported in dynamic analysis of wrap faced walls [24] and segmental facing walls [23]. The contour of incremental octahedral shear strain within soil is shown in Fig. 7. The highest strain develops near the end of reinforcement. The shear strains are developed near within reinforced zone and also extended to the unreinforced backfill soil. From the shear strain contour and comparative graph of horizontal and vertical displacements and incremental octahedral shear strain within the backfill soil, schematic of deformation zones is shown in Fig. 8.

Soil strains and reinforcement strains are analyzed in terms of incremental stains developed during dynamic excitation, to establish influence of strain variation on
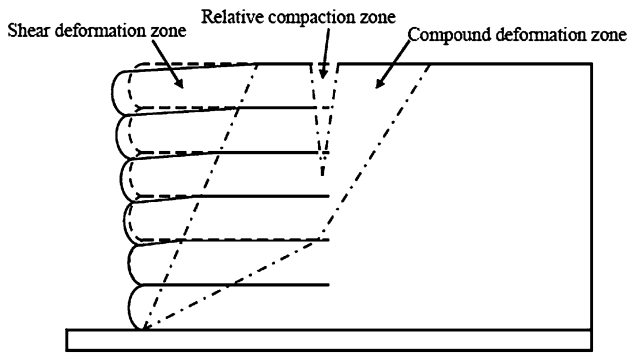
Fig. 8 Schematic of deformation zones in wrap faced reinforced soil retaining wall after dynamic excitation

deformation zones. Figure 9 presents variations of incremental octahedral shear strains ($\Delta\gamma_{oct}$) in the soil and incremental axial strain ($\Delta\varepsilon_{a\_rein}$) in reinforcement layers along length of the wall. The incremental octahedral shear strains ($\Delta\gamma_{oct}$) reduce to negligible values at distance of 8.0 m from facing at elevations 6.0 m denoting maximum mobilization of unreinforced backfill beyond reinforced soil zone. The incremental octahedral shear strain ($\Delta\gamma_{oct}$) reduces to negligible value at distance of 7.0 m and 6.0 m from facing at elevations 5.0 m and 4.0 m respectively. The compound deformation zones extend to deeper unreinforced backfill at higher elevations.

From the figure it is also observed that incremental axial strains ($\Delta\varepsilon_{a\_rein}$) after dynamic excitation are less than 2 % at top three layers (top, 5th and 4th layer) of reinforcement. At these elevations whole reinforcement length is located within the maximum strained zone of soil due to deeper

extension compound zone into unreinforced backfill, as a result insignificant strain increments are noticed within reinforcement. In the 1st layer of reinforcement which is extended to the zone of negligible soil strain, i.e., beyond 2.0 m from the facing, the strain increment is 2.8 % at a distance of 0.8 m from facing. Moreover, the overburden pressure on reinforcement increases with increasing depth of reinforcement layers. So the friction developed on reinforcement at lower layers is more than that of top layers. From the above observations, it is noticed that during dynamic excitation, the reinforcement strain increments are affected by the extent compound deformation zone into unreinforced backfill soil and friction developed on reinforcement due to overburden pressures.
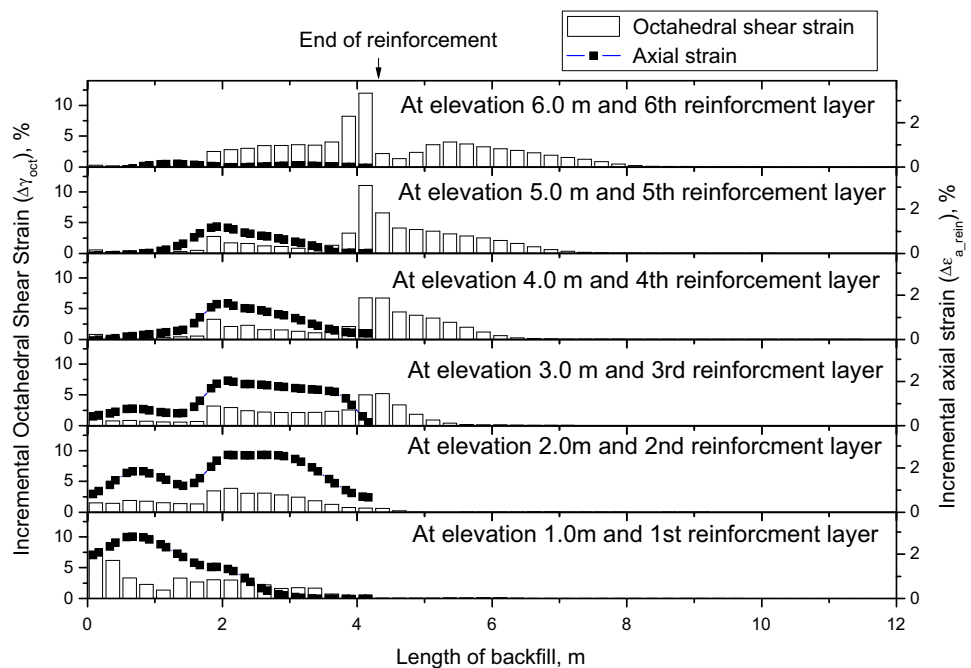
Parametric Studies

Parametric studies are conducted to observe increments of octahedral shear strain of soil and reinforcement strain during dynamic excitation. Reinforcement length (L_{rein}), number of reinforcing layers (N_L) and type of backfill (friction angle, ϕ) are varied in different simulations. The parameters considered for these parametric studies are listed in Table 2.

Effect of Reinforcement Length

Three different lengths of reinforcements 0.7H, 1.0H and 1.2H, where H is height of wall, are considered. All other model parameters were kept same as discussed in earlier

Fig. 9 Incremental octahedral shear strain in soil element and incremental axial strain in reinforcement ($a = 0.2$ g, $f = 3$ Hz, $L_{rein}/H = 0.7$, $N_L = 6$)

Table 2 List of parameters considered for parametric studies

| Soil properties	
Friction angles (ϕ), degrees	30, 38, 43
Reinforcement configuration	
Length of reinforcement (L_{rein})	0.7H, 1.0H, 1.2H
No of reinforcing layers (N_L)	4, 6, 8

section. Figure 10 shows the comparison of incremental octahedral shear strains ($\Delta\gamma_{oct}$) in backfill soil with different reinforcement lengths after 20 cycles of dynamic excitation of 0.2 g acceleration at 5 Hz frequency. The maximum incremental octahedral shear strains are 9.7, 4.7 and 2.2 % near the end of reinforcement at elevation 6.0 m for wall with reinforcement lengths 0.7H, 1.0H and 1.2H, respectively. The incremental octahedral shear strains ($\Delta\gamma_{oct}$) within soil are lesser for wall with longer reinforcement at higher elevations (4.5 and 6.0 m). The length of compound deformation zone measured from end of reinforcement is 3.75, 2.0 and 1.3 m at elevation 5.5 m for wall with reinforcement lengths 0.7H, 1.0H and 1.2H, respectively. Compound deformation zone length gradually decreases with decrease in elevations and becomes zero beyond elevation 3.5 m. It is also observed that at lower elevations (<2.5 m) soil strain variations are insignificant for different reinforcement lengths considered.

Variations of incremental axial strain in reinforcement ($\Delta\varepsilon_{a\_rein}$), after dynamic excitation for model walls with different reinforcement lengths, at different elevations, are shown in Fig. 11. The maximum incremental axial strain ($\Delta\varepsilon_{a\_rein}$) at first layer of reinforcement (1.5 m elevation)

are 2.8, 2.5 and 2.3 % for walls with reinforcement length of 0.7H, 1.0H and 1.2H, respectively. This indicates higher reinforcement strain for model wall with shortest reinforcement length. With increase in elevation, it is seen that reinforcement strains for longer reinforcements are higher than that for shorter reinforcement lengths. The reinforcement strain increments are within 2.5 and 2.0 % for second and third layer of reinforcement for wall with reinforcement length 0.7H and 1.2H, while that of fifth layer of reinforcement is 1.2 and 1.4 % respectively. The reinforcement strain increment in top layer are minimum (<0.5 %) for wall with different reinforcement lengths. From comparison of results it is observed, wall with longest reinforcement length have least compound deformation zone and reinforcement strains are more at higher layers. At higher elevations the compound deformation zone length is higher for wall with shorter reinforcement length causing more displacement of soil and reinforcement together, causing lesser increment of reinforcement strain. The compound deformation zone is smaller for wall with longer reinforcement causing less displacement of soil and reinforcement together, resulting in more strain development in reinforcement. With the observations presented here are also to be interpreted as using longer reinforcement lengths at higher elevations (up to half the height of wall) and the remaining with shorter reinforcement lengths balances strain levels and lead to get the optimum benefit of reinforcement capacities.

From the above results it can be stated that change in the reinforcement length doesn't affect the length of deformation zone with the retained backfill. However the

Fig. 10 Comparison of octahedral shear strain at backfill of wrap faced wall with reinforcement length 0.7H, 1.0H and 1.2H ($a = 0.2$ g, $f = 5$ Hz and $N_L = 6$)
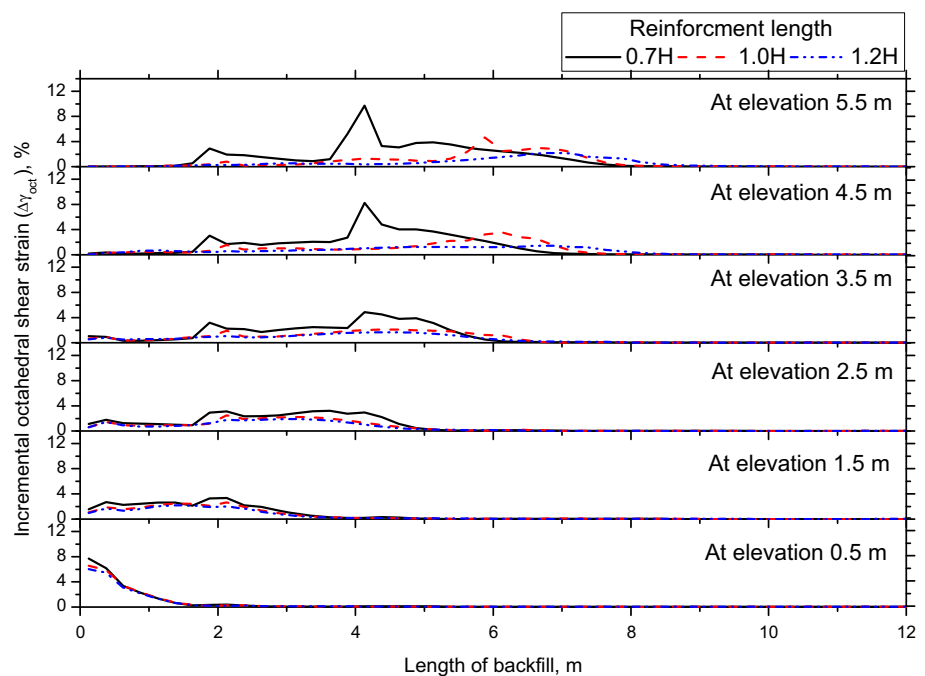
Fig. 11 Incremental axial strain in reinforcment with L_{rein}/H = 0.7, 1.0 and 1.2 (a = 0.2 g, f = 5 Hz, N_L = 6)
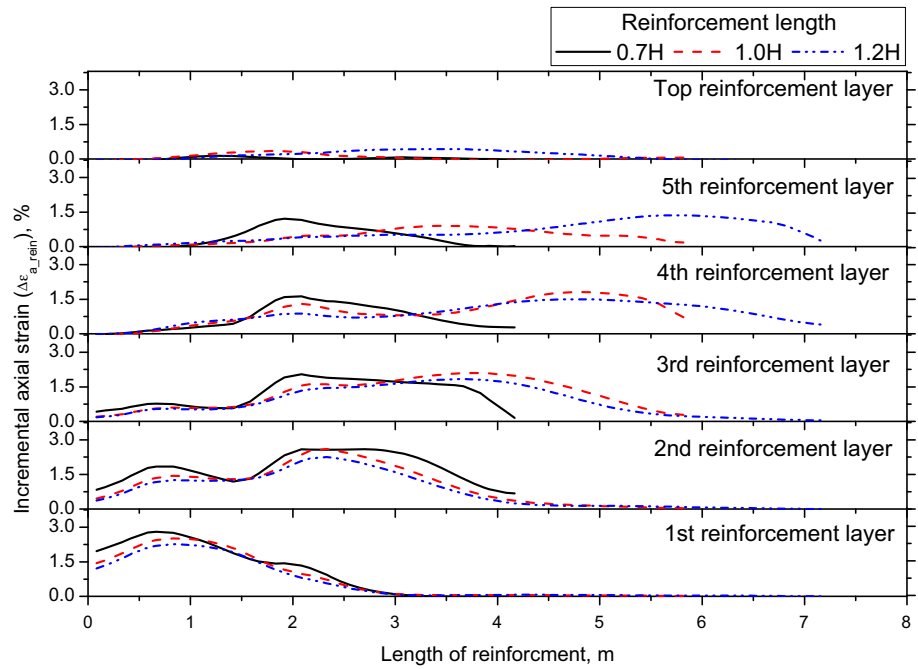

magnitude of octahedral shear strains and wall displacements are reduced considerably with increase in reinforcement length 0.7H to 1.0H. But for 1.2H reinforcement length the benefit is not proportional. Further it is also observed that at the lower elevations the soil strains and reinforcement strains were not significantly affected by change in reinforcement length. So providing longer reinforcements up to 1/3–1/2 the height of wall would yield better performance results.

Effect of Number of Reinforcing Layers

Three different reinforcing layer configurations, 4, 6 and 8 layers were considered keeping the reinforcement length (L_{rein}) constant at 0.7H. Comparison of incremental octahedral shear strains ($\Delta\gamma_{oct}$), after dynamic excitation (a = 0.2 g, f = 5 Hz), for wrap faced walls with different reinforcing layers is shown in Fig. 12. Incremental octahedral strains ($\Delta\gamma_{oct}$) near the face of wall are very low in

Fig. 12 Comparison of octahedral shear strain in soil with 4, 6 and 8 layers of reinforcement (a = 0.2 g, f = 5 Hz and L_{rein}/H = 0.7)
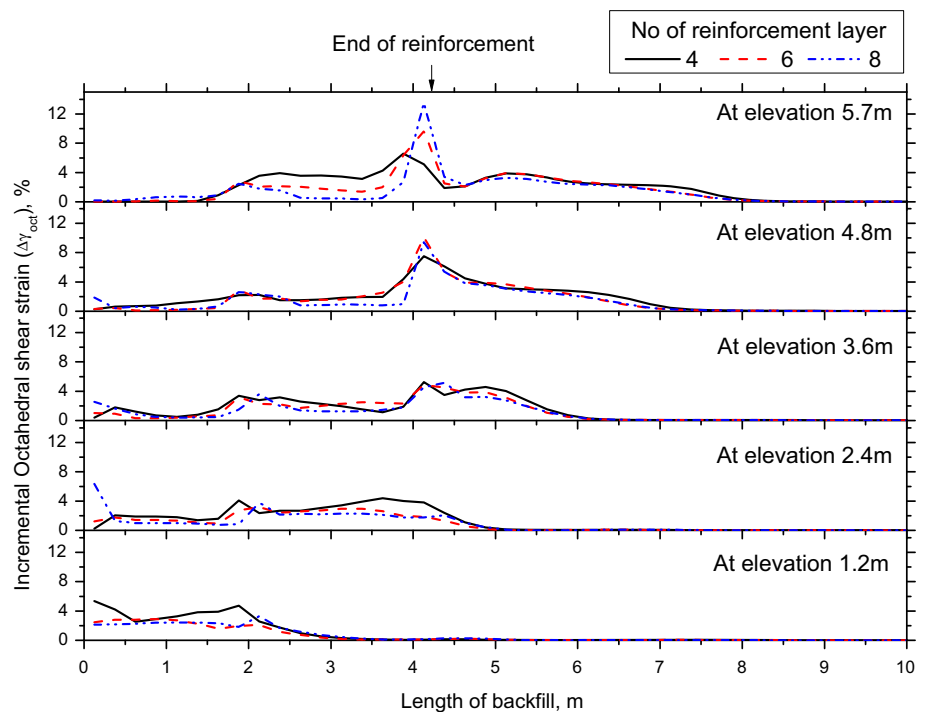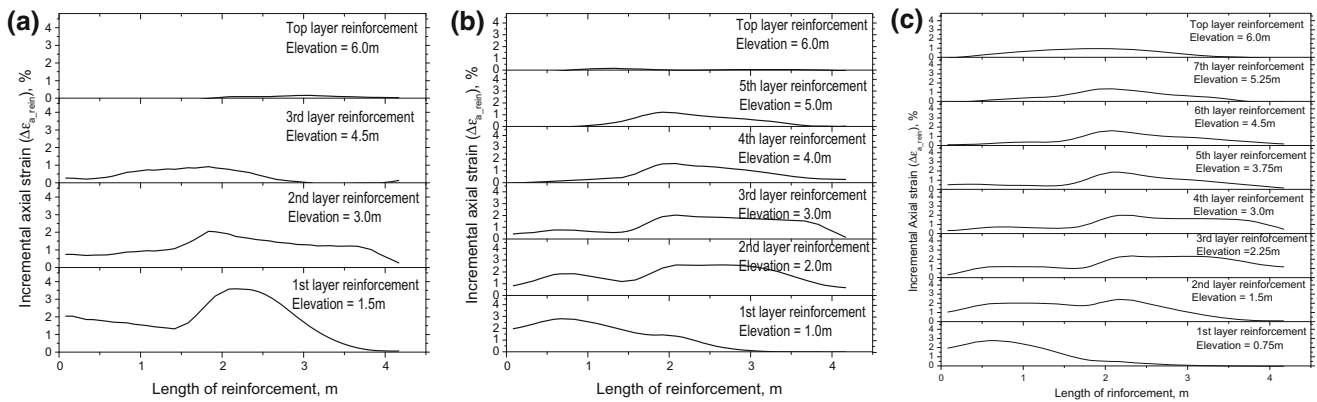
Fig. 13 Incremental axial strain in reinforcement ($a = 0.2$ g, $f = 5$ Hz, $L_{rein}/H = 0.7$) with different number of reinforcement layers (N_L) **a** $N_L = 4$ **b** $N_L = 6$; and **c** $N_L = 8$

the order of less than 2 % at higher elevations (5.7, 4.8 and 3.6 m) for all three different reinforcement layer configurations. But the strain values increase gradually to higher values near end of the reinforcement (4.2 m from facing) from a distance of about 1.5 m from face of wall. Highest strain value of 12 % was observed for 8 layer configuration at 5.7 m elevation near end of reinforcement. The incremental octahedral shear strains ($\Delta\gamma_{oct}$) after the reinforcement zone decreases gradually to zero at distance of 8 m from face of wall. The strains variation beyond the zone of peak strain values is almost same for all different layer configurations.

The variation of reinforcement axial strain increments ($\Delta\varepsilon_{a\_rein}$) after dynamic excitation for walls with 4, 6 and 8 layers of reinforcement are shown in Fig. 13. The reinforcement strain increments ($\Delta\varepsilon_{a\_rein}$) at top layer are nearly 0.2 and 1.0 % at elevation 6.0 m for wall with 4 and 8 layers of reinforcement, respectively. But the average incremental octahedral shear strain ($\Delta\gamma_{oct}$) within the reinforcement zone (Fig. 12) are 3.6 and 0.5 %, respectively, for 4 and 8 layers of reinforcement at the same elevation. Similarly with the octahedral shear strain increments ($\Delta\gamma_{oct}$) of 1.2 and 0.95 % for wall with 4 and 8 layers of reinforcement at elevation 4.8 m, the reinforcement strain increments ($\Delta\varepsilon_{a\_rein}$) are 0.8 and 1.6 %, respectively. The reinforcement axial strain increments are influenced similarly in lower elevations by the octahedral shear strain at that elevation. The incremental octahedral shear strain decreases in soil with increase in number of reinforcing layers and the corresponding axial strain increment in reinforcements increases during dynamic excitation. Increase in number of reinforcement layers, gives more stiffness to the soil which effectively decrease the octahedral shear strains. At higher elevations reinforcement strains are more for wall with more reinforcing layers due to more stiffness in reinforced zone.

Effect of Backfill Soil (Angle of Internal Friction)

Different types of backfills, in terms of different friction angles, 30°, 38° and 43° are considered, subjected to 20 cycles of dynamic excitation of 0.2 g acceleration at 5 Hz frequency. Figure 14 shows the comparison of incremental octahedral shear strain ($\Delta\gamma_{oct}$) in the backfill of the three model walls, after the dynamic excitation. The length of compound deformation zones beyond the end of reinforcement is 4.8, 3.8 and 3.3 m at elevation 5.5 m for walls with backfill friction angles of 30°, 38° and 43° respectively. The extent of compound deformation zones gradually decrease with decrease in elevations of backfill and reduce to zero at elevation 1.5 and 0.5 m. The length of compound deformation zone decreases with increase in backfill friction angle at higher elevations. This indicates lesser soil movement for backfill with higher friction angle.

The variations of reinforcement strain increments ($\Delta\varepsilon_{a\_rein}$) after dynamic excitation along the reinforcement length for walls with different backfill soils are shown in Fig. 15. The reinforcement strain increments are more in the upper four reinforcement layers of reinforcement for wall with backfill friction angle of 43°. This is due to lesser displacement of soil and reinforcement towards facing and more interaction between soil and reinforcement due to high interface friction angles. The extent compound deformation zones is maximum for wall with backfill friction angle 30° denoting more mobilization of soil and reinforcement towards the front facing and lesser reinforcement strains developed.

Response of Designed Wrap Faced Wall

Hypothetical configurations of wrap faced reinforced soil walls are considered in earlier sections for observing the

Fig. 14 Comparison of octahedral shear strain at backfill with different friction angles: 30°, 38° and 43° ($a = 0.2$ g, $f = 5$ Hz and $N_L = 6$)
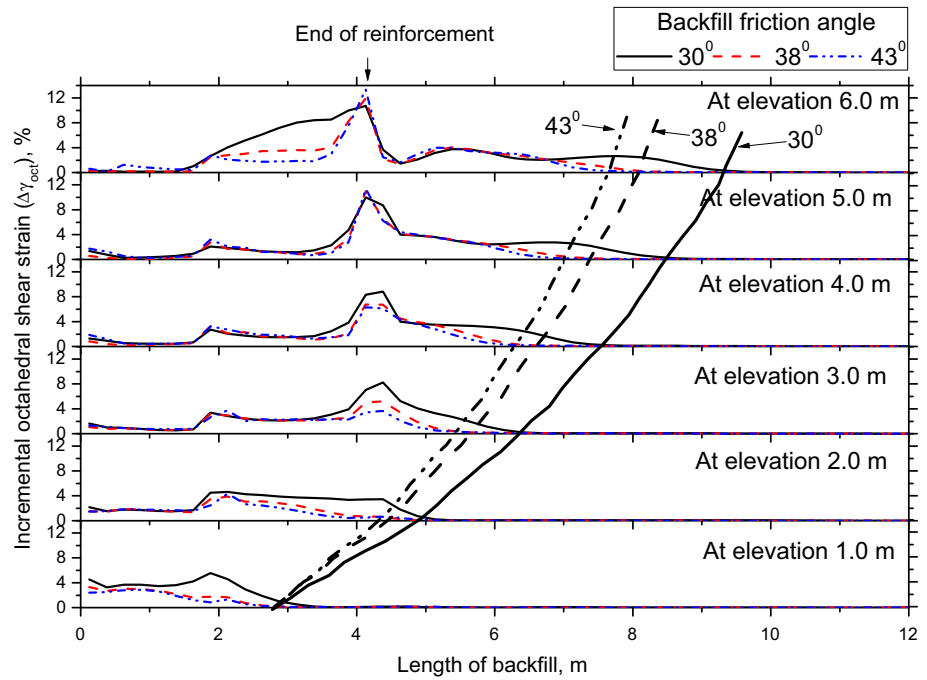
Fig. 15 Incremental axial strain in reinforcement with backfill friction angle 30°, 38° and 43° ($a = 0.2$ g, $f = 5$ Hz, $N_L = 6$)
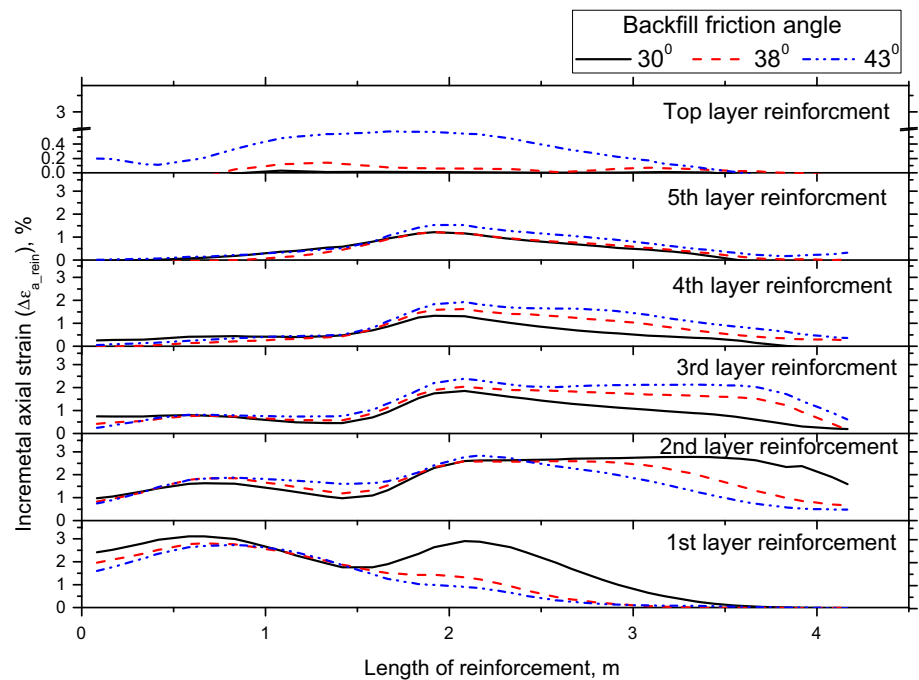

interdependency of soil strains, reinforcement strain and deformation zones. It is observed from the study that development of shear strains are influenced the formation of deformation zones. The strains on reinforcements are influenced by the soil reinforcement interaction and extent of compound deformation zone at backfill. To observe the influence of soil and reinforcement strains on wall response, a 6 m high wrap faced wall is designed considering [FHWA [7]] recommendations (maximum spacing of 400 mm between reinforcement layers and minimum

reinforcement length of 0.7H. Hence, the spacing between reinforcement layers as 400 mm and length of reinforcement as 0.7H are adopted. The material parameters considered for the design are same as that of hypothetical wrap faced walls. Calculations for stability check stability checks were performed for static case and dynamic case (design acceleration = 0.2 g) that are presented in Table 3. Figure 16 shows the octahedral shear strain, horizontal and vertical displacements along the length of backfill after end of dynamic excitation of 5 Hz frequency and 0.2 g

Table 3 Stability check results for the designed wall

Capacity demand ratio		Eccentricity		T_{max}		T_r	$L_{required}$, m		$L_{provided}$, m
Static	Dynamic	Static	Dynamic	Static	Dynamic		Static	Dynamic	
1.39	1.36	1.43	2.04	11.44	11.92	12.11	1.36	1.37	4.2

Fig. 16 Octahedral shear strain, horizontal displacement and vertical displacement along the length of backfill ($a = 0.2$ g, $f = 5$ Hz, $L_{rein}/H = 0.7$, $N_L = 15$)
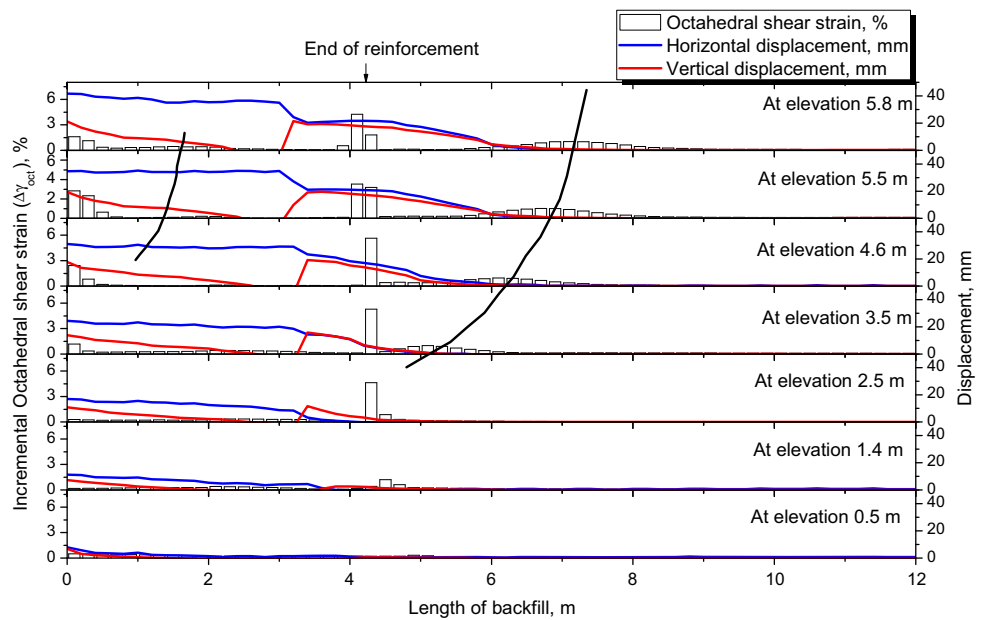
Fig. 17 Incremental axial strains in reinforcement layers ($a = 0.2$ g, $f = 5$ Hz, $N_L = 15$)
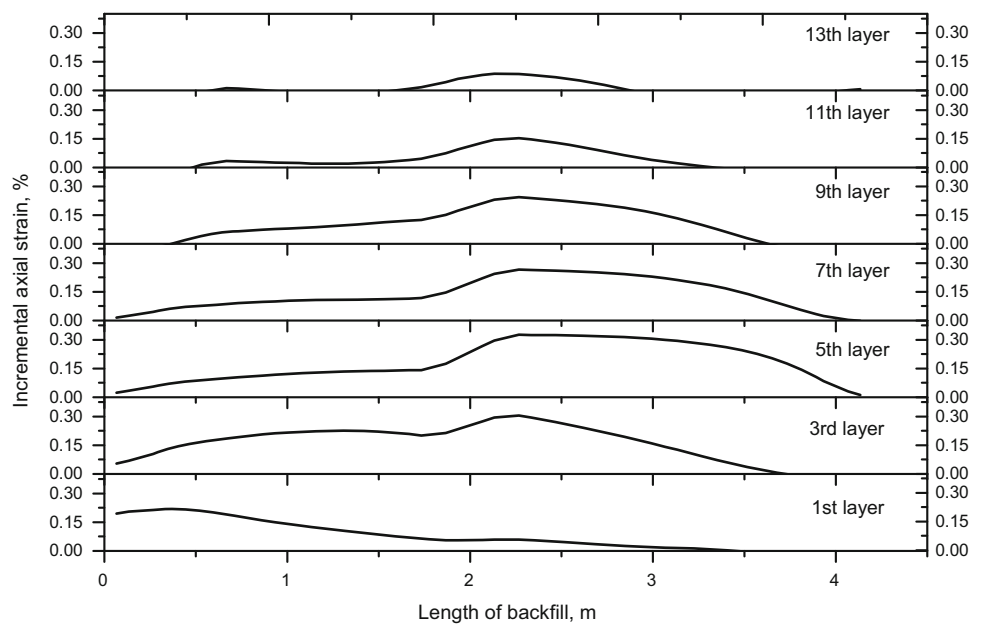
acceleration. The horizontal displacement of soil element near the face of wall is 41.7 mm at an elevation of 5.5 m and remains almost constant up to 3.0 m from face of wall. The horizontal displacement then decreases and become almost zero at 7.0 m from the face of wall. The vertical displacement of soil element is 21.3 mm near the face of

wall at that elevation. The vertical displacement decrease to zero within reinforced zone. The maximum vertical displacement of 21.5 mm is near the end of reinforcement. The vertical displacement decreases to zero at a distance of 7.0 m from the facing. The octahedral shear strains near the face of wall are about 2 % above 2.5 m elevation. The

maximum octahedral shear strains are in the range of 4 to 5 % near the end of reinforcement at elevations 5.8 and 2.5 m. However, the shear strains within the reinforced zone are lesser in the order of 0.51. The formation of compound deformation zone at backfill is observed. Comparing the horizontal and vertical displacement and octahedral shear strain it is observed that a shear deformation zone is observed within backfill soil, zone of relative compaction formed at end of reinforcement and compound deformation zone is observed at unreinforced backfill. The incremental reinforcement strains after dynamic excitation at different elevations are shown in Fig. 17. The axial strain increments during dynamic excitation are within 0.5 %. From the figure maximum strain increments are observed in lower layers of reinforcement. The axial strain increments in upper layer are less due to lesser overburden pressure and formation of compound deformation zone within backfill soil.

Conclusions

Numerical model studies are conducted to observe the variation of octahedral shear strain in soil and reinforcement strain during dynamic excitation. The following conclusions are made from the present study.

(a) The deformation of warp faced reinforced soil wall is due to three distinct modes of failure surfaces—shear deformation within reinforced zone, relative compaction near end of reinforcement and compound failure surface extending to backfill zone.

(b) The shear deformation within reinforced zone is due to horizontal movement of soil element towards the face of wall. The relative compaction near the end of reinforcement is due to due to vertical settlement. The compound deformation within backfill is due to horizontal movement of a part of retained zone along with the reinforced zone.

(c) The deformation due to relative compaction near end of reinforcement and compound deformation zone can be restricted by increasing the reinforcement length.

(d) The shear deformation within the reinforced zone can be reduced by increasing the number of reinforcing layers.

(e) Extent of the compound deformation zone in the retained zone is mainly affected by the type of backfill (friction angle). Lesser friction angle (softer backfill) showed deeper deformation zones.

(f) The strains developed in reinforcements are influenced by strain developed within soil element, extent of compound deformation zone into deep backfill and interaction between soil and reinforcement.

References

1. Bhattacharjee A, Murali Krishna A (2012) Development of numerical model of wrap faced walls subjected to seismic excitation. Geosynth Int 19(5):354–369. doi:10.1680/gein.12.00022
2. Burke C, Ling HI, Liu H (2004) Seismic response analysis of a full scale reinforced soil retaining wall, Proc. 17th ASCE Engineering Mechanics conference, June 13–16, 2004, pp 1–6
3. Cai Z, Bathurst RJ (1995) Seismic response analysis of geosynthetic reinforced soil segmental retaining walls by finite element method. Comput Geotech 17:523–546
4. Duncan JM, ByrneP, Wong KS, Mabry P (1980) Strength, stress, strain and bulk modulus parameters for finite element analyses of stresses and movements in soil masses. Report No. UCB/GT/80-01, Department of Civil Engineering, University of California, Bekrley
5. El-Emam MM, Bathurst RJ (2004) Experimental design, instrumentation and interpretation of reinforced soil wall response using shaking table test. Int J Phys Model Geotech 4(4):13–32
6. FHWA (2001) Mechanically stabilized earth walls and reinforced soil slopes design and construction guidelines. Publication No. FHWA-NHI-00-043, US Department of Federal Highway Administration (FHWA)
7. FHWA (2010) Mechanically Stabilized earth walls and reinforced soil slopes design and construction guidelines. Publication No. FHWA-NHI-10-024,FHWA GEC 011- Volume I, US Department of Federal Highway Administration (FHWA)
8. Hatami K, Bathurst RJ (2000) Effect of structural design on fundamental frequency of reinforced-soil retaining walls. Soil Dyn Earthq Eng 19(3):137–157
9. Huang CC, Wu SH (2007) Simplified approach for assessing seismic displacement of soil retaining walls. Part II : Geosynthetic-reinforced walls with rigid panel facing. Geosynth Int 14(5):264–276
10. Itasca (2008). Fast Lagrangian analysis of Continua3D Version 3.0, Itasca Consulting Group Inc., Minneapolis
11. IRC (2010). Four-laning of highways through public private partnership – manual of specifications & standards. Indian Roads Congress, New Delhi
12. Kramer SL (1996) Geotechnical earthquake engineering. Prentice Hall, Upper Saddle River, NJ 653
13. Krishna AM, Latha GM (2012) Modeling of dynamic response of wrap faced reinforced soil retaining wall. Int J Geomech, ASCE 12(4):439–450
14. Krishna AM, Latha GM (2009) Seismic behavior of rigid-faced reinforced soil retaining wall models: reinforcement effect. Geosynth Int 16(5):364–371
15. Krishna AM, Latha GM (2007) Seismic response of warp-faced reinforced soil-retaining wall models using shaking table tests. Geosynth Int 14(6):355–364
16. Kuhlemeyer RL, Lysmer J (1973) Finite element method accuracy for wave propagation problems. J Soil Mech Found Div ASCE 99(SM5):421–427
17. Latha GM, Krishna AM (2008) Seismic response of reinforced soil retaining wall models: influence of backfill relative density. Geotext Geomembr 26(4):335–349
18. Lee KZZ, Chang NY, Ho HY (2010) Numerical simulation of geosynthetic-reinforced soil walls under seismic shaking. Geotext Geomembr 28:317–334
19. Ling HI, Leshchinsky D (2003) Finite element parameter studies of the behavior of segmental block reinforced soil retaining walls. Geosynth Int 10(3):77–94
20. Ling HI, Liu H, Mohri Y (2005) Parametric studies on the behavior of reinforced soil retaining walls under earthquake loading. J Eng Mech, ASCE 131(12):1056–1065

21. Ling HI, Liu H, Kaliakin VN, Leshchinsky D (2004) Analyzing dynamic behavior of geosynthetic-reinforced soil retaining walls. J Geotech Geoenviron Eng ASCE 130(8):911–920

22. Liu H (2009) Analyzing the reinforcement loads of geosynthetics-reinforced soil walls subject to seismic loading during service life. J Perform Constr Facil ASCE 23(5):292–302

23. Liu H, Wang X, Song E (2011) Reinforcement load and deformation mode of geosynthetics-reinforced soil walls subject to seismic loading during service life. Geotext Geomembr 29:1–16

24. Liu H, Ling HI (2012) Seismic response of reinforced soil retaining walls and strain-softening of backfill soil. Int J Geomech ASCE 12(4):351–356

25. Ramakrishnan S, Budhu M, Britto A (1998) Laboratory seismic tests on geotextile wrap-faced and geotextile-reinforced segmental retaining walls. Geosynth Int 5(1–2):55–71

26. Sakaguchi M, Yamada K, Tanaka M (1994) Prediction of deformation of geotextile reinforced soil walls subjected to earthquakes. Proc. of the 5th international conference on geotextiles, geomembranes and related products, Singapore, September 1994, Vol. 1, pp 521–524

27. Zarnani S, Bathurst RJ (2009) Influence of constitutive model on numerical simulation of EPS seismic buffer shaking table tests. Geotext Geomembr 27(4):308–312